ORIGINAL PAPER

Ali Reza Keshavarzi · Ali Reza Gheisi

Stochastic nature of three dimensional bursting events and sediment entrainment in vortex chamber

Abstract In this study, three dimensional quadrant analysis of bursting process was used to recognize the susceptible regions for sediment entrainment and deposition at the bed of a vortex chamber. From the analysis, it was found that two dimensional quadrant analysis in unable to find the turbulent coherent structure of flow near the bed of the vortex chamber. Therefore, a new method based on three dimensional bursting process is introduced in this study to define the turbulent flow structure. Based on the new methodology in this study, the bursting event is divided into eight different cube zones according to three dimensional velocity fluctuations. It was realized that, four cube zones interactions are toward the central orifice of the vortex chamber and four cube zones interactions are toward the wall of the chamber and they are categorized as classes A and B, respectively. The results from the experiments showed that in class A, the internal sweep events (class IV-A) moves the settled sediment particles toward the central orifice of the chamber, whereas in class B the external sweep events (class IV-B) moves the settled sediment particles toward the external region of the chamber. Also the transition probabilities of the bursting events in 64 particular movements were determined. The result showed that stable organizations of each class of the events had highest transition probabilities whereas cross organizations had lowest transition probabilities. Additionally, an effort was made to find the average inclination angle of the three dimensional bursting events in each cube zone. The results showed that near the bed of the vortex chamber by increasing the tangential velocity toward the center of the chamber, the average inclination angle of the events in the cube zones decreased. Also, at the region where the sediment particles were deposited, the inclination angles had higher values.

A. R. Keshavarzi (✉) · A. R. Gheisi
Water Department, Shiraz University, Shiraz, Iran
E-mail: keshavrz@shirazu.ac.ir
Tel.: +98-711-228-6130
Fax: +98-711-228-6130

Keywords Vortex chamber · 3-D bursting events · Inclination angle · Sediment entrainment

1 Introduction

The structure of flow in vortex settling chamber is complicated and fully three dimensional. The vortex chamber is a self-flushing settling basin during the operation and comparing to the usual settling basin, it is very efficient and economical. In vortex chamber, the flow circulates in a cylindrical chamber and generates secondary currents inside the flow. Little studies have previously been conducted to understand the flow structure inside the vortex chamber. However, due to complexity and stochastic nature of turbulence, the structure of turbulent flow is not completely understood.

The concept of bursting process and its contribution in turbulent shear stress was firstly introduced by Kline et al. (1967) as a quasi-periodic process by which the momentum is transferred into the boundary layer. The bursting process consists of four different types of events, according to quadrant analysis of two dimensional velocity fluctuations and they are classified as: outward interaction ($u' > 0$, $v' > 0$), ejection ($u' < 0$, $v' > 0$), inward interaction ($u' < 0$, $v' < 0$) and sweep ($u' > 0$, $v' < 0$), in quadrant zones 1, 2, 3 and 4, respectively. In order to define sediment entrainment function with the effect of bursting events, Nychas et al. (1973); Drake et al. (1988); Thorne et al. (1989); Nelson et al. (1995); Keshavarzi (1997) and Keshavarzi and Ball (1997, 1999) pointed out that the sweep event is mostly responsible for sediment entrainment from the bed. Also in the studies by Nezu and Nakagawa (1993); Nakagawa and Nezu (1978) and Hinze (1975), it was concluded that in turbulent flow, the bursting event is the major process for transfer of momentum and they are very effective for sediment entrainment and transport. Grass (1971) and Nakagawa and Nezu (1978) pointed out the contributions of sweep and ejection events for sediment entrainment and deposition are more than outward and

inward interactions. Keshavarzi and Ball (1997, 1999); Thorne et al. (1989); Nakagawa and Nezu (1993); Townsend (1956) and Yalin (1992) found that the occurrence of sweep and ejection events is more than outward and inward interactions. Keshavarzi (1997) pointed out that in sweep event the average magnitude of the shear stress is much higher than the time averaged shear stress. Offen and Kline (1975); Keshavarzi and Ball (1999) and Papanicolaou et al. (2002) introduced different models to define particles entrainment with the inclusion of the bursting process. Also, to define the stochastic nature of bursting process, Keshavarzi and Shirvani (2002) used Markov process to find the organization of the occurrence of the bursting process and they found that the first order Markov process is an appropriate model to define the occurrence of the bursting process. Additionally they classified the movement of the events as; stable, marginal and cross organizations and they found that the stable organization is the most probable event. Additionally, Yen (2002) pointed out that to model sediment transport accurately, it is necessary to incorporate the bursting events in the modeling of turbulent flow and sediment entrainment function. Most previous studies were performed in open channel with two dimensional quadrant analyses of velocity fluctuations. However, in spite of the importance of three dimensional coherent structures and in particular the bursting events in the vortex chamber their characteristics have not been investigated sufficiently in detail. In this paper, the characteristics of three dimensional bursting processes inside the vortex chamber along with transition probabilities of the events in each class were computed at any particular movement from the experimental data. Also the inclination angle of each event is reported in this paper.

2 Experimental setup

The experiments in this study were carried out in a physical model in the laboratory. The model was built with the diameter of $D = 1.00$ m, and height of $H = 0.70$ m. In this study the experiments were conducted in counter clock flow condition. Under this condition, the angular distance from the inlet channel to the outlet overflow weir was about 270°. A diaphragm was also installed at $h_1 = 0.17$ m from the inlet channel bed at the periphery of the basin. The width of the inlet canal was 0.20 m with the slope of 0.01. A flushing pipe was installed at the center of the chamber with a diameter of 0.05 m. The basin bed was sloped at $S_c = 0.10$ into the central flushing orifice and the chamber depth at its periphery was $h_2 = 0.06$ m with the weir length of $L_1 = 0.50$ m. A schematic diagram of the chamber is shown in Fig. 1.

A three-dimensional downward facing Acoustic Doppler Velocity meter (Micro-ADV, SonTek) was used to measure the velocity of flow in tangential, vertical and radial directions. The Micro-ADV has the advantages of
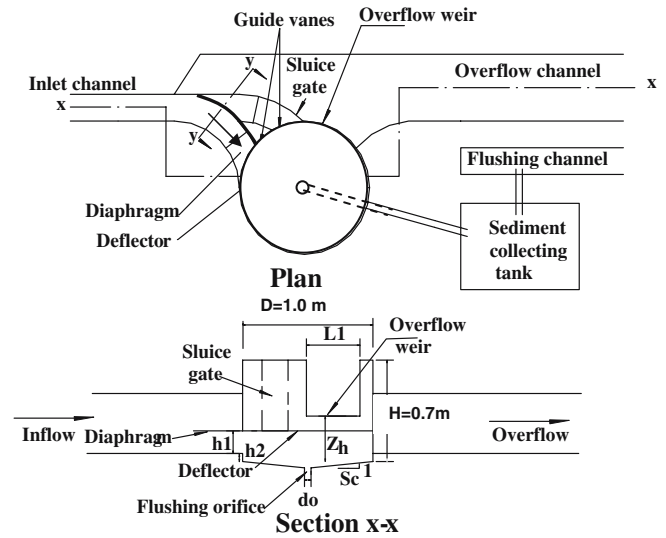

Fig. 1 Schematic diagram of physical model used in the experiments

measuring three components of velocity fluctuations simultaneously and being suitably strong to be used in the intensive vortex chamber flow. Additionally only minimal disturbance is made to the flow as the sampling volume is remote from the instrument and no calibration is required (Sontek 1997). The ADV uses the Doppler technique to measure the velocity of small particles in the water. When operating close to the bottom of vortex chamber, the ADV can reliably operate well near the boundary. The acoustic transmitters of the ADV were oriented inside the vortex chamber and it simultaneously measured the velocity components in tangential, vertical and radial directions as shown in Fig. 2. Data acquisition was started after reaching to the steady flow condition within the vortex chamber. The ADV measures velocities to an accuracy of ± 0.1 mm/s in full scale, if the water salinity and temperature are correctly determined
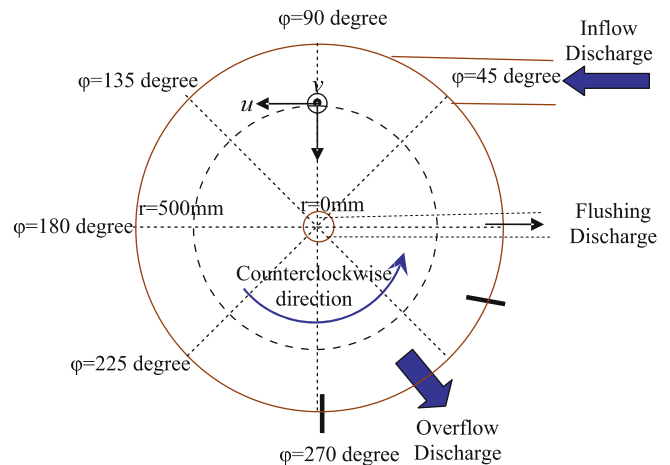

Fig. 2 Plan view of the vortex chamber and coordinate system of velocity measurement

(Sontek 1997). To reduce the inaccuracies, the water salinity and temperature were measured during the experimental test. The velocity was measured with a sampling rate of 50 Hz. The duration of sampling was 120 s and totally 6000 samples at each point were captured. The velocity of flow was measured at 48 different nodal points, at eight angles and six circular lines at a distance of 2 cm from the bed of vortex chamber. The sediment particle was fed into the inlet canal just at the inlet of the chamber at water surface. The particle size distribution of the sediment used in this study is shown in Fig. 3.

3 Result and discussions

In the vortex chamber, the secondary current and centrifugal force of the flow are used to exclude sediment particles from the diverted water. The secondary currents develop inside the chamber as a result of the flow deceleration at the bottom of the chamber. These secondary currents move the fluid layer toward the bed of the chamber and finally deflect it into the central flushing orifice. During the operation of vortex chamber, some specific pattern of sediment deposition will be formed on the bed of chamber. An example of sediment deposition pattern is shown in Fig. 4a. The sediment deposition pattern at the bed of vortex chamber indicates the action of secondary currents at the bed. The sediment pattern consists of a region near the periphery wall of the chamber, which starts from the inlet orifice and extends toward the overflow weir. In this region a great amount of sediment is piled up (see Fig. 4b). It shows that this region is susceptible for sediment accumulation. In recent studies for example Keshavarzi and Ball (1999) it is shown that the coherent structure of turbulent flow and in particular bursting events are responsible for sediment entrainment and it was found the sweep event occurred more frequently than other events. It exerts forces to the sediment particles and causes them to move by rolling, sliding and occasionally saltating in stream wise flow direction. Similarly, the ejection event has been recogniz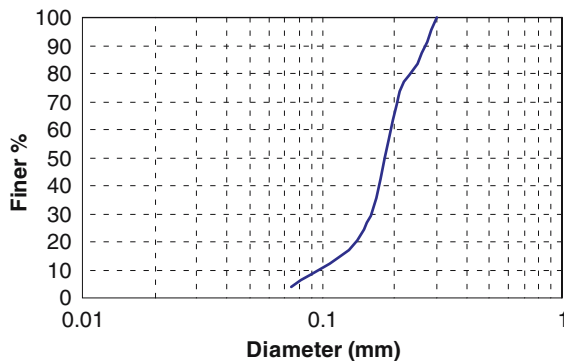ed to be responsible for suspended sediment transport because it maintains the sediment particles in suspension. Therefore, in this study it is attempted to use two and three dimensional quadrant analysis of bursting events for identifying the susceptible regions of sediment entrainment and deposition at the bed of vortex chamber.

3.1 Analysis of two dimensional bursting events

Initially the velocity fluctuations in vertical and tangential directions were computed based on the following relationships as;
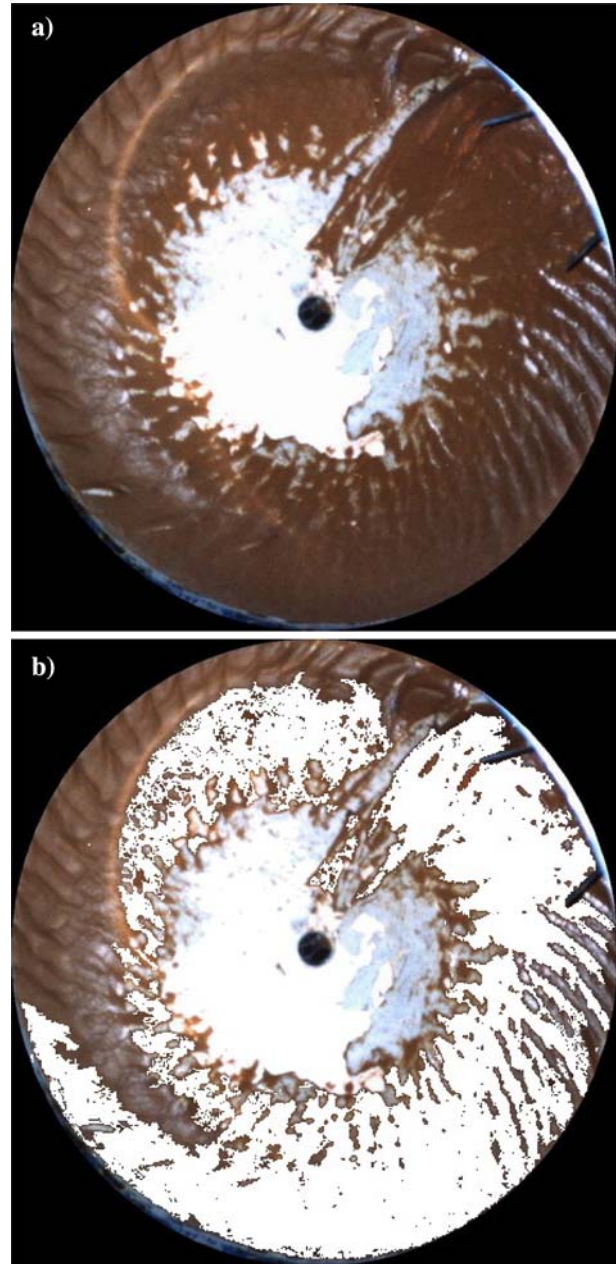

Fig. 4 Pattern of sediment deposition on the bed of vortex chamber

Fig. 3 Grain size distribution of the sediment particles used in this experimental study

$$v' = v - \bar{v} \text{ and } u' = u - \bar{u} \tag{1}$$

Where v and u are the instantaneous velocities in the vertical and tangential directions and $\bar{v}$ and $\bar{u}$ are the temporal mean velocities in the vertical and tangential directions, respectively. The temporal mean velocities are also given by

$$\bar{v} = \frac{1}{N}\sum_{i=1}^{N} v_i \text{ and } \bar{u} = \frac{1}{N}\sum_{i=1}^{N} u_i \tag{2}$$

Where N is the number of instantaneous velocity samples. According to two dimensional bursting process the velocity fluctuations (events) are categorized in quadrant zones 1, 2, 3 and 4 respectively. Here, the contribution probability of the events in each bursting quadrant is determined by

$$P_k = \frac{n_k}{N} \tag{3}$$

Where P_k is the contribution probability of each event, n_k is the number of occurrences of each event, N is the total number of events and the subscript represents the individual quadrants ($k = 1$–4). The probabilities of the events in each quadrant are computed from the experimental data and are shown in Fig. 5. A comparison was made between the distribution of contribution probability of events in each quadrant near the bed and the pattern of sediment deposition at the bed of the chamber. It was found that there is no agreement between the regions of entrained sediment and sweep and ejection events in the bed of vortex chamber.

Therefore, in this study an attempt was made to compute the contribution probability of events in each quadrant on the basis of velocity fluctuations in vertical and radial directions. As a result, the velocity fluctuations in radial direction were computed by following relationships as

$$\omega' = \omega - \bar{\omega} \text{ and } \bar{\omega} = \frac{1}{N}\sum_{i=1}^{N} \omega_i \tag{4}$$

Where, ω is the instantaneous velocity fluctuation, and $\bar{\omega}$ is the temporal mean velocities in the radial direction, respectively, and their relevant contribution probabilities are shown in Fig. 6. Similarly no agreement was found between the regions of entrained sediment with sweep and ejection events in the bed of vortex chamber.

Additionally, from the velocity fluctuations in vertical, tangential and radial directions, the Reynolds turbulent shear stress in tangential and radial directions on a horizontal plane near the bed were determined using

$$\overline{v'u'} = \frac{1}{N}\sum_{i=1}^{N} v'_i u'_i \tag{5}$$

$$\tau_t = -\rho\overline{v'u'} \tag{6}$$

$$\overline{v'\omega'} = \frac{1}{N}\sum_{i=1}^{N} v'_i \omega'_i \tag{7}$$

$$\tau_r = -\rho\overline{v'\omega'} \tag{8}$$

$$\vec{\tau}_{\text{total}} = \vec{\tau}_t + \vec{\tau}_r \tag{9}$$

The value of Reynolds shear stress in tangential direction (Eq. 6), radial direction (Eq. 8) and total Reynolds shear stress vector (Eq. 9) on the horizontal plane near the bed of the chamber were determined for each point and they are shown in Fig. 7. As a result, it was found that based on velocity fluctuations in radial direction, the total Reynolds shear stress vector is highly deflected from the tangential direction and the turbulent structure near the bed is completely three dimensional. Therefore, the result showed that the two dimensional bursting events is unable to define the turbulent coherent structure of the flow near the bed of the chamber. To find the rate of deviation of velocity fluctuations from the tangential direction, the inclination angle of the trend line from the tangential direction is determined and it is shown in Fig. 8. The inclination angle for the bed of the vortex chamber is also shown in Fig. 9. It was found that this deviation occurs in the range of $\pm 35°$ from the tangential direction. Therefore, in this study a new method was defined for the definition of bursting events in three dimensions near the bed of the chamber with consideration of the velocity fluctuations in three dimensions according to defined coordinate system in Fig. 2.

3.2 Analysis of three dimensional bursting events

In this study, the velocity fluctuations are classified into two sets of bursting events including internal and external clusters, according to quadrant analysis of the data. Hence, the bursting events are categorized into two clusters, according to the sign of the velocity fluctuations in three dimensions. Class A represents the clusters events which deflect toward the internal direction of the chamber and class B represents the cluster events which deflect toward the external direction of the chamber. Therefore, the bursting process consists of four groups in class A and four groups in class B. The three dimensional velocity fluctuations (u', v', ω') are defined as the variation from the temporal mean velocities in the tangential, vertical and radial directions, respectively. Algebraically, they are defined as:

$$u' = u - \bar{u}, v' = v - \bar{v} \text{ and } \omega' = \omega - \bar{\omega} \tag{10}$$

Where u, v and ω are the instantaneous velocities in the tangential, vertical and radial directions and $\bar{u}$, $\bar{v}$ and $\bar{\omega}$ are the temporal mean velocities in tangential, vertical and radial directions, respectively.

As a result, the classes A and B of bursting events are identified are defined as

- Cubic Zone 1: Internal outward interaction or class I-A, ($u' > 0$, $v' > 0$, $\omega' > 0$)
- Cubic Zone 2: Internal ejection or class II-A, ($u' < 0$, $v' > 0$, $\omega' < 0$)

Fig. 5 Contribution probability of the events in quadrant I–IV based on two dimensional bursting processes in tangential and vertical direction at the bed of vortex chamber
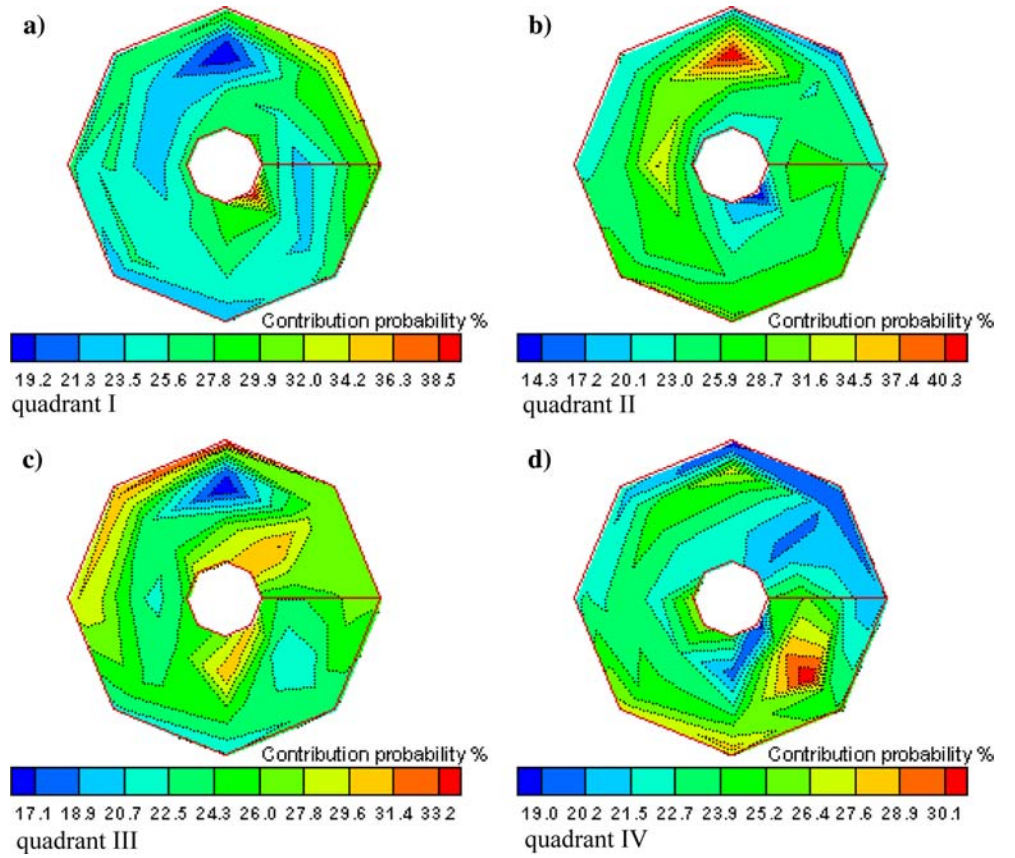
a)

b)

Contribution probability %

19.2 21.3 23.5 25.6 27.8 29.9 32.0 34.2 36.3 38.5
quadrant I

Contribution probability %

14.3 17.2 20.1 23.0 25.9 28.7 31.6 34.5 37.4 40.3
quadrant II

c)

d)

Contribution probability %

17.1 18.9 20.7 22.5 24.3 26.0 27.8 29.6 31.4 33.2
quadrant III

Contribution probability %

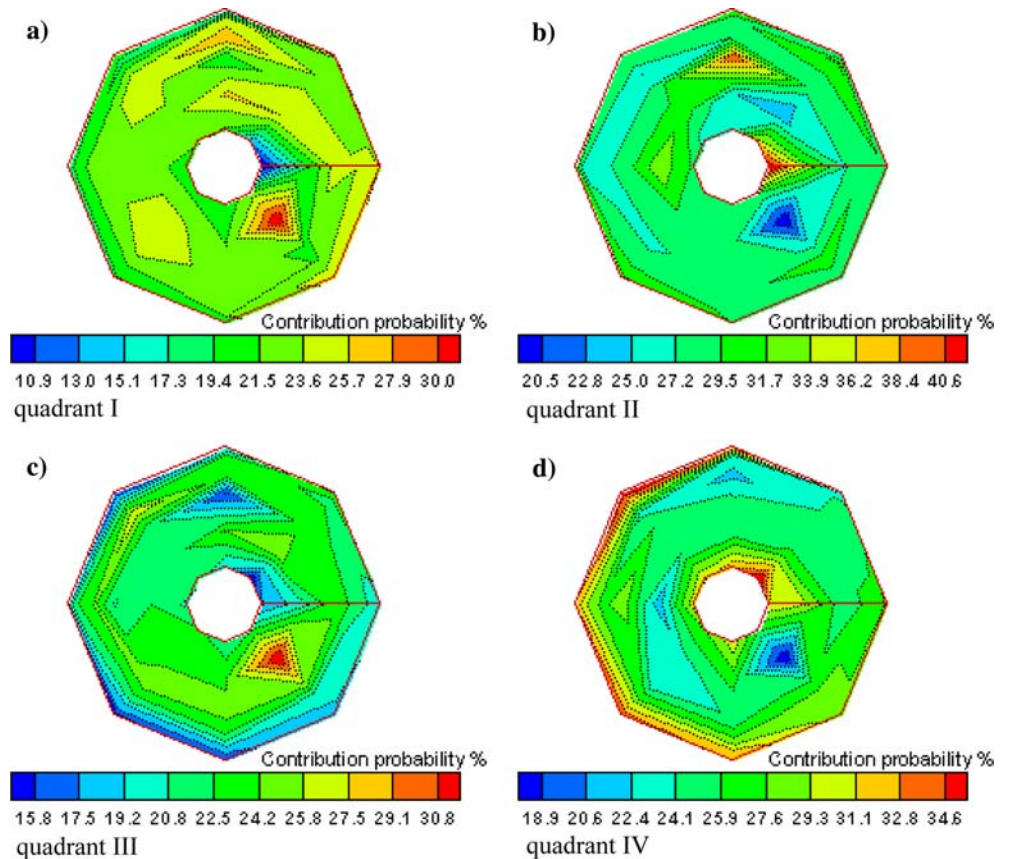19.0 20.2 21.5 22.7 23.9 25.2 26.4 27.6 28.9 30.1
quadrant IV

Fig. 6 Contribution probability of the events in quadrant I–IV based on two dimensional bursting processes in radial and vertical direction at the bed of vortex chamber
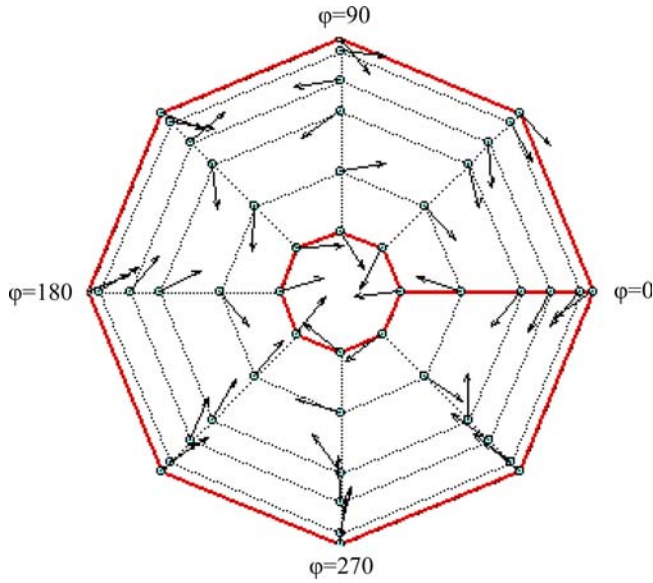
a)

b)

Contribution probability %

10.9 13.0 15.1 17.3 19.4 21.5 23.6 25.7 27.9 30.0
quadrant I

Contribution probability %

20.5 22.8 25.0 27.2 29.5 31.7 33.9 36.2 38.4 40.6
quadrant II

c)

d)

Contribution probability %

15.8 17.5 19.2 20.8 22.5 24.2 25.8 27.5 29.1 30.8
quadrant III

Contribution probability %

18.9 20.6 22.4 24.1 25.9 27.6 29.3 31.1 32.8 34.6
quadrant IV

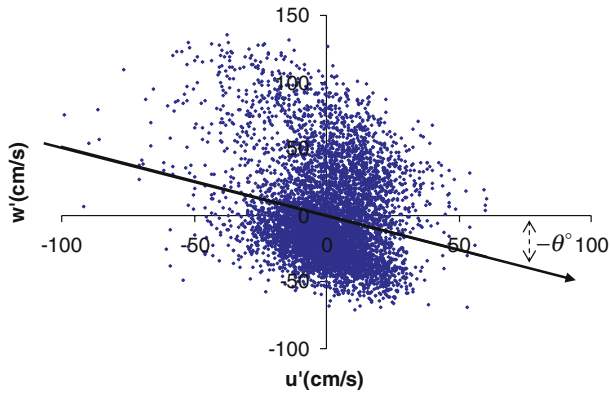**Fig. 7** Direction of the Reynolds shear stress vectors near the bed of the chamber

Fig. 8 Angular deviations of the velocity fluctuations trend line from the tangential direction
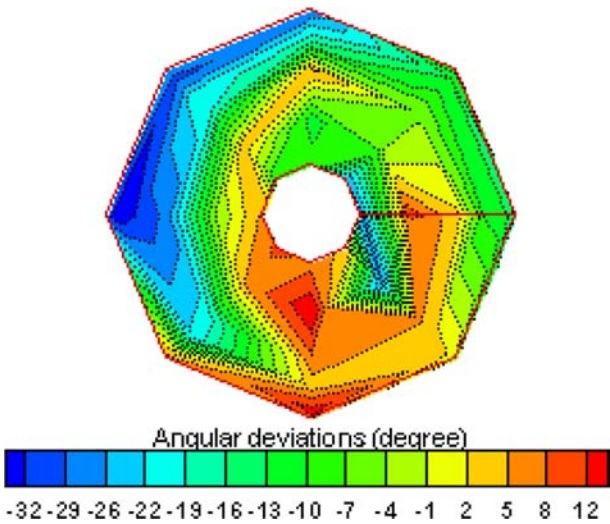

Fig. 9 Computed angular deviations of the trend lines from the tangential direction at the bed of vortex chamber

- Cubic Zone 3: Internal inward interaction or class III-A, ($u' < 0$, $v' < 0$, $\omega' < 0$)
- Cubic Zone 4: Internal sweep or class IV-A, ($u' > 0$, $v' < 0$, $\omega' > 0$)
- Cubic Zone 5: External outward interaction or class I-B, ($u' > 0$, $v' > 0$, $\omega' < 0$)
- Cubic Zone 6: External ejection or class II-B, ($u' < 0$, $v' > 0$, $\omega' > 0$)
- Cubic Zone 7: External inward interaction or class III-B, ($u' < 0$, $v' < 0$, $\omega' > 0$)
- Cubic Zone 8: External sweep or class IV-B, ($u' > 0$, $v' < 0$, $\omega' < 0$)

An example of velocity fluctuations in three dimensions is shown in Fig. 10. The above classes are responsible for momentum transfer between horizontal adjacent layers of water flow and produce the instantaneous turbulent shear stress along the tangential and radial directions.

### 3.3 Contribution probability of the events in 3-D bursting events

Based on the three dimensional bursting process the instantaneous shear stress is divided into eight different classes. In this approach the contribution probability (frequency) of events in each bursting class is determined by

$$P_k = \frac{n_k}{N} \tag{11}$$

$$N = \sum_{k=1}^{8} n_k \tag{12}$$

Where P is the frequency of each event class, n_k is the number of occurrences of each event class, N is the total number of events and the subscript represents the individual class ($k = 1$–8). Based on the above relationships the contribution probability of three dimensional bursting events in each class was determined for each point separately and they are shown in Fig. 11a–h. It was found that at the region where a great amount of sediment is piled up, the contribution probability of the events in bursting classes of I-B, II-B, III-B and IV-B is more than other regions and in particular the external sweep event (class IV-B), that causes the settled sediment particles to move toward the external space of the chamber. However, exactly at this location the contribution probability of the events in bursting classes of I-A, II-A, III-A and IV-A which acts toward the internal space of the chamber, is less than other regions. The internal sweep events (class IV-A) that make the settled sediment particles move toward the internal space of the chamber. It was found that the excluded sediment particles by the vortex settling chamber performance will be led to the central orifice by means of internal sweep events (class IV-A). The external sweep events (class IV-B) will lead the sediment particles toward the periphery wall of the chamber and cause them to be

Fig. 10 An example of the velocity time series from the experiment
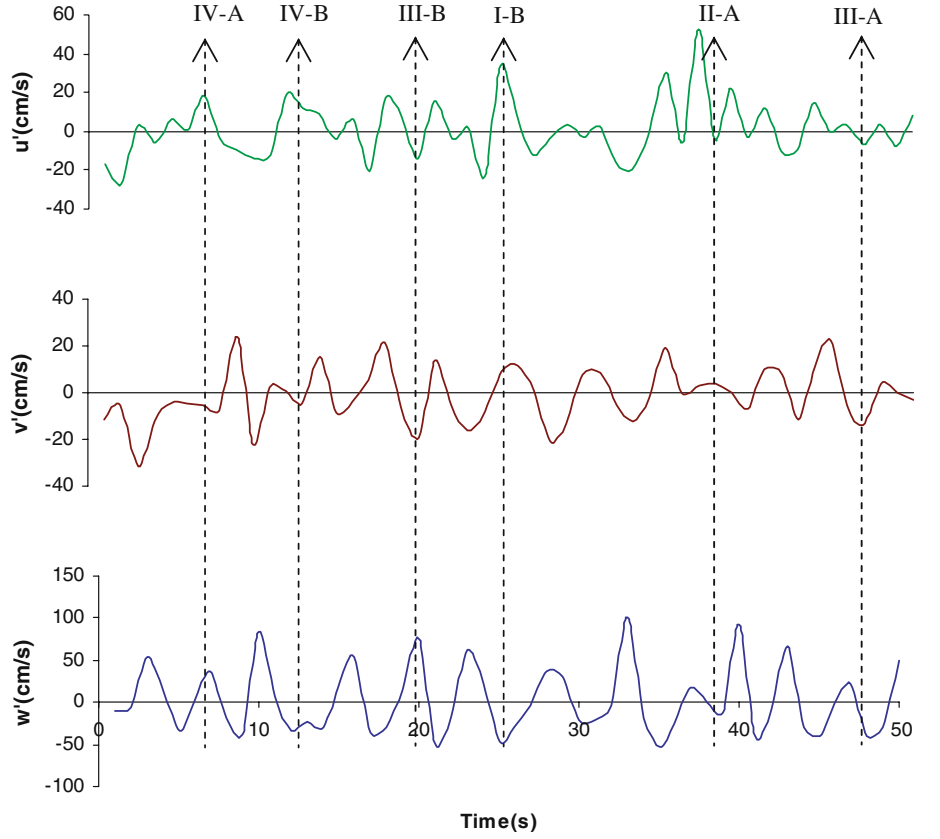
piled up near the chamber's wall. It was also attempted to find a relationship between the values of contribution probability of eight bursting classes. By using statistical analysis it was found that the best correlation will be obtained within the elements of bursting classes type A and B separately. The proposed relationships are shown in Table 1. It confirms the new proposed method for event classification of class A and B in three dimensional bursting process. Also the average contribution probability of the bursting event classes at the bed of the chamber is shown in Fig. 12.

3.4 Transition probability of bursting processes

Three dimensional bursting processes consist of a sequential occurrence of discrete events which is classi-fied in eight zones. In this study, the change of events from current situation to the next situation in a time series is defined as movement. Here, the transition probabilities of the movement of the events from one zone to the next zone at each point are computed by the following formula:

$$P_{i \Rightarrow j} = \frac{n_{i \Rightarrow j}}{n_i} \quad i, j = 1, 2, 3, 4, 5, 6, 7, 8 \tag{13}$$

Where; $n_{i \Rightarrow j}$ is the number of event transition from zone i at time (t) to zone j at time $(t+1)$ and n_i is the number of events in zone i in the time series followed by another event, hence $n_i = n_{i \Rightarrow 1} + n_{i \Rightarrow 2} + n_{i \Rightarrow 3} + n_{i \Rightarrow 4} + n_{i \Rightarrow 5} + n_{i \Rightarrow 6} + n_{i \Rightarrow 7} + n_{i \Rightarrow 8}$.

Therefore based the above definition 64 cases of tran-sition probabilities can be recognized. The elements of transition probabilities are shown in the following matrix:

$$P(I) = \begin{vmatrix} P_{1 \Rightarrow 1} & P_{1 \Rightarrow 2} & P_{1 \Rightarrow 3} & P_{1 \Rightarrow 4} & P_{1 \Rightarrow 5} & P_{1 \Rightarrow 6} & P_{1 \Rightarrow 7} & P_{1 \Rightarrow 8} \\ P_{2 \Rightarrow 1} & P_{2 \Rightarrow 2} & P_{2 \Rightarrow 3} & P_{2 \Rightarrow 4} & P_{2 \Rightarrow 5} & P_{2 \Rightarrow 6} & P_{2 \Rightarrow 7} & P_{2 \Rightarrow 8} \\ P_{3 \Rightarrow 1} & P_{3 \Rightarrow 2} & P_{3 \Rightarrow 3} & P_{3 \Rightarrow 4} & P_{3 \Rightarrow 5} & P_{3 \Rightarrow 6} & P_{3 \Rightarrow 7} & P_{3 \Rightarrow 8} \\ P_{4 \Rightarrow 1} & P_{4 \Rightarrow 2} & P_{4 \Rightarrow 3} & P_{4 \Rightarrow 4} & P_{4 \Rightarrow 5} & P_{4 \Rightarrow 6} & P_{4 \Rightarrow 7} & P_{4 \Rightarrow 8} \\ P_{5 \Rightarrow 1} & P_{5 \Rightarrow 2} & P_{5 \Rightarrow 3} & P_{5 \Rightarrow 4} & P_{5 \Rightarrow 5} & P_{5 \Rightarrow 6} & P_{5 \Rightarrow 7} & P_{5 \Rightarrow 8} \\ P_{6 \Rightarrow 1} & P_{6 \Rightarrow 2} & P_{6 \Rightarrow 3} & P_{6 \Rightarrow 4} & P_{6 \Rightarrow 5} & P_{6 \Rightarrow 6} & P_{6 \Rightarrow 7} & P_{6 \Rightarrow 8} \\ P_{7 \Rightarrow 1} & P_{7 \Rightarrow 2} & P_{7 \Rightarrow 3} & P_{7 \Rightarrow 4} & P_{7 \Rightarrow 5} & P_{7 \Rightarrow 6} & P_{7 \Rightarrow 7} & P_{7 \Rightarrow 8} \\ P_{8 \Rightarrow 1} & P_{8 \Rightarrow 2} & P_{8 \Rightarrow 3} & P_{8 \Rightarrow 4} & P_{8 \Rightarrow 5} & P_{8 \Rightarrow 6} & P_{8 \Rightarrow 7} & P_{8 \Rightarrow 8} \end{vmatrix}$$

Fig. 11 Contribution
probability of the events in zone
1–8 based on three dimensional
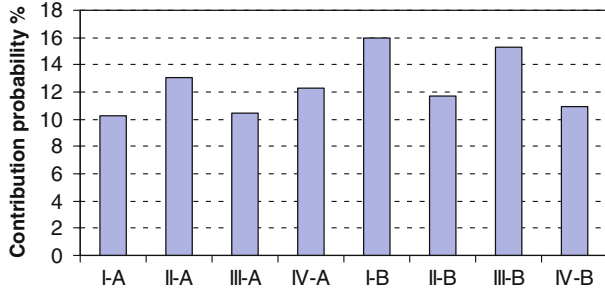bursting process at the bed of
vortex chamber
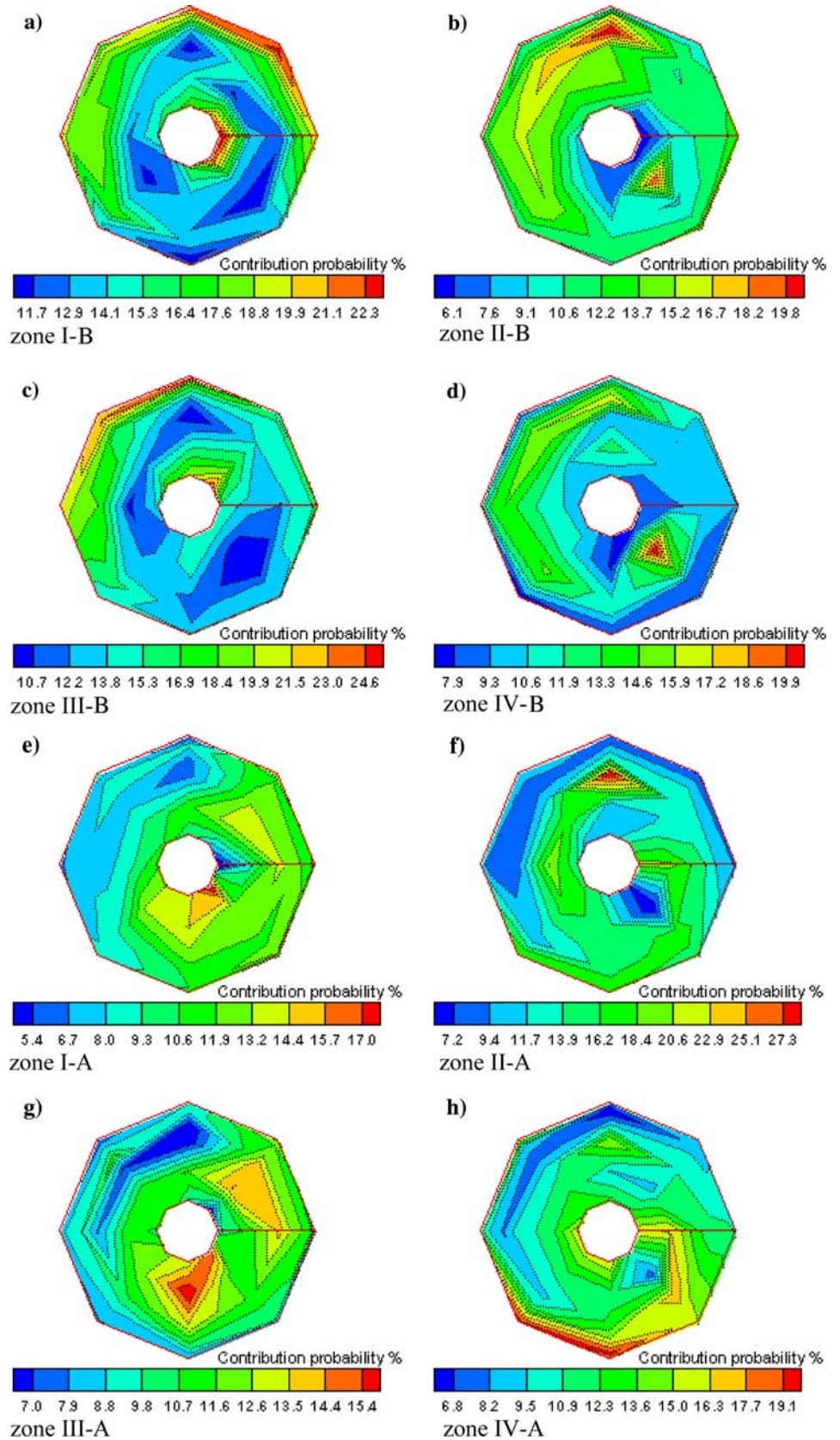
The above definition was applied to the situation of events at each point where velocity fluctuations were measured and the transition probabilities of bursting events were determined. Therefore, 64 transition probabilities for each point near the chamber bed were identified. It was found that the stable organizations of the events have

Table 1 Proposed relationship between the contribution probability of the events in eight bursting classes

Proposed relationships of class type A	R^2
$P_{I-A} = -1.13 - 0.17 P_{II-A} + 0.98 P_{III-A} + 0.28 P_{IV-A}$	0.73
$P_{II-A} = 2.21 - 0.77 P_{I-A} + 0.67 P_{III-A} + 0.96 P_{IV-A}$	0.51
$P_{III-A} = 4.23 + 0.73 P_{I-A} + 0.11 P_{II-A} - 0.22 P_{IV-A}$	0.72
$P_{IV-A} = 6.04 + 0.68 P_{I-A} + 0.52 P_{II-A} - 0.72 P_{III-A}$	0.55

Proposed relationships of class type B	R^2
$P_{I-B} = 7.15 - 0.4 P_{II-B} + 0.6 P_{III-B} + 0.4 P_{IV-B}$	0.5
$P_{II-B} = 3.27 - 0.28 P_{I-B} + 0.17 P_{III-B} + 0.95 P_{IV-B}$	0.65
$P_{III-B} = 3.31 + 0.78 P_{I-B} + 0.32 P_{II-B} - 0.38 P_{IV-B}$	0.47
$P_{IV-B} = 2.22 + 0.19 P_{I-B} + 0.66 P_{II-B} - 0.14 P_{III-B}$	0.63

Fig. 12 Average contribution probability of the events in zone 1–8 at the bed of vortex chamber based on three dimensional bursting process

higher transition probabilities. For example movement of $[I - A \Rightarrow I - A]$, $[II - A \Rightarrow II - A]$, $[III - A \Rightarrow III - A]$, $[IV - A \Rightarrow IV - A]$, $[I - B \Rightarrow I - B]$, $[II - B \Rightarrow II - B]$, $(III - B \Rightarrow III - B)$ and $[IV - B \Rightarrow IV - B]$ have the highest transition probability. Also the following movements of events have the least transition probabilities $[I - A \Leftrightarrow III - A]$, $[II - A \Leftrightarrow IV - A]$, $[I - B \Leftrightarrow III - B]$, $[II - B \Leftrightarrow IV - B]$ and they are the least possible movements. Therefore, the distribution of transition probability of the highest probable movements at the bed of the chamber is plotted on the bed of vortex chamber and they are shown in Fig. 13a–h. Also the transition probabilities were averaged for 48 points near the bed and are shown in Table 2. It was found that at the location where the sediment particles were accumulated the stable organization of class type B such as $[I - B \Rightarrow I - B]$, $[II - B \Rightarrow II - B]$, $[III - B \Rightarrow III - B]$, $[IV - B \Rightarrow IV - B]$ is more probable than others.

3.5 Angle of the events

The force exerted to sediment particles on the chamber bed during events of internal and external sweep zones (classes IV-A & IV-B) depends upon the inclination angle of the velocity fluctuations which is called angle of attack. Therefore, in this study the average inclination of the velocity fluctuations from horizontal plane in external and internal sweep zones and also the other zones is computed by the following method:

Table 2 Average transition probability for 64 particular movements near the bed of vortex chamber

	External outward interaction (t+1)	External ejection (t+1)	External inward interaction (t+1)	External sweep (t+1)	Internal outward interaction (t+1)	Internal ejection (t+1)	Internal inward interaction (t+1)	Internal sweep (t+1)
External outward interaction (t)	56.27	2.63	0.87	13.22	8.55	12.26	3.70	2.50
External ejection (t)	4.63	49.38	12.62	1.52	12.11	12.65	3.61	3.48
External inward interaction (t)	1.19	13.25	58.11	2.58	3.57	2.90	7.47	10.92
External sweep (t)	14.17	1.65	4.78	46.86	3.68	3.73	12.56	12.55
Internal outward interaction (t)	16.01	11.56	3.58	4.47	45.10	3.45	1.24	14.59
Internal ejection (t)	16.76	9.72	2.76	3.76	2.49	51.40	12.28	0.83
Internal inward interaction (t)	4.70	4.30	14.09	11.77	1.19	13.26	47.62	2.70
Internal sweep (t)	3.17	3.47	16.14	9.23	12.00	0.88	2.43	52.68

Fig. 13 Transition probability of the highest probable movements at the bed of the chamber
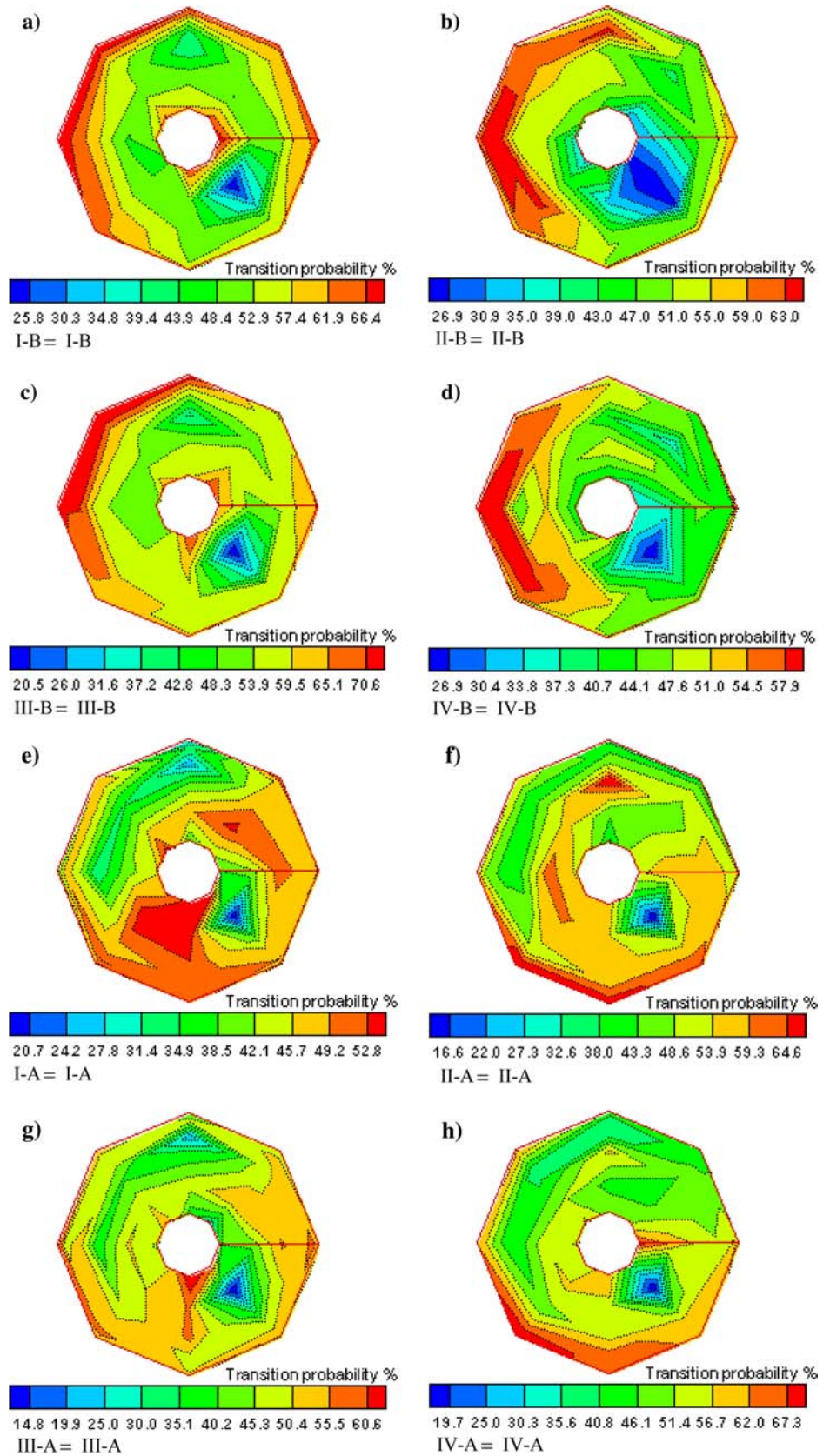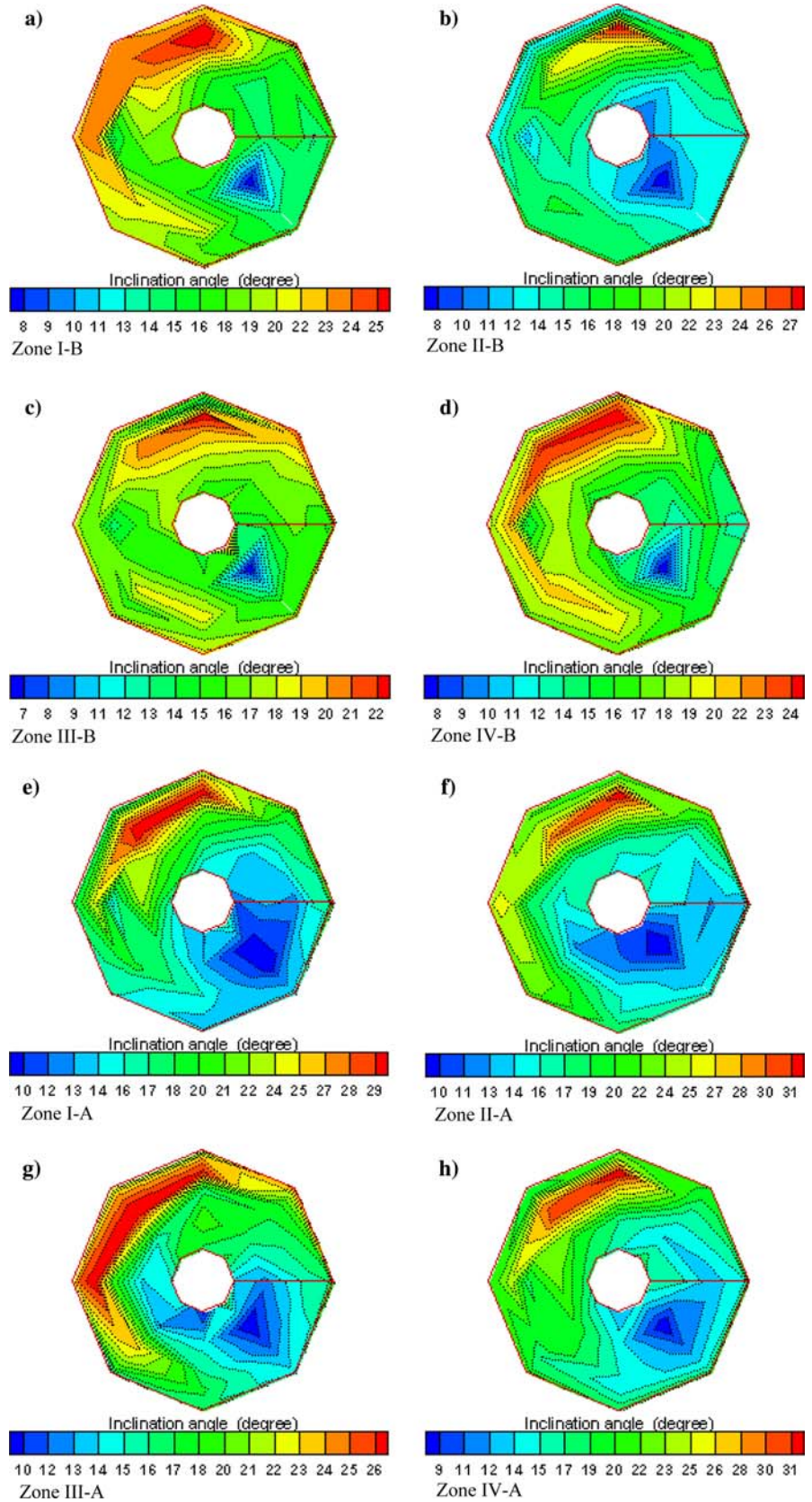
Fig. 14 Inclination angle of three dimensional bursting events in each zone at the bed of vortex chamber

$$\theta_i = \left| \arctan\left(\frac{v'}{\sqrt{(u'^2 + \omega'^2)}} \right) \right| \qquad (14)$$

Where θ_i is the angle of inclination from the horizontal plane in zone i for each three dimensional bursting events. To transform the data into a normally distributed, the Box-Cox power transformation (see Box-Cox 1964) was applied to the computed inclination angles in each zone. Then the transformed values were averaged and the inverse Box-Cox transformation was applied to the mean value to determine the mean inclination angle of each zone separately.

Therefore, based on the above method the average inclination angle of the bursting events in each zones (1–8) were determined for each point near the bed of the chamber. The inclination angle of each zone was plotted and are shown in Fig. 14a–h. It was found that at the region where a great amount of sediment is deposited, the bursting events have the highest inclination from the horizontal plane. This fact was more noticeable about the zones of class type A, which acts toward the internal space of the chamber. It was also tried to find a relationship between the inclination angles of eight bursting zones. Using statistical analysis, it was concluded that the best correlation will be obtained within the inclination angles of bursting zones type A and B, separately. The proposed relationships are shown in Table 3. It also confirms the new proposed method of event classification in three dimensional bursting processes. The above Table shows that the inclination angle of one zone depends on the inclination angle of the other zone which acts in the same direction toward the internal space of the chamber or external space of the chamber. The average inclination angle of the bursting events from horizontal plane in each zone near the chamber bed is shown in Fig. 15. In addition, the average inclination angles of each zone at corresponding radius from the center of the chamber were computed separately. These values were plotted against the radial distance from center of the chamber and they are shown in Fig. 16. As the distance increase from the center of the chamber, the value of the inclination angle will increase until the radius becomes 35 cm. After this distance the value will
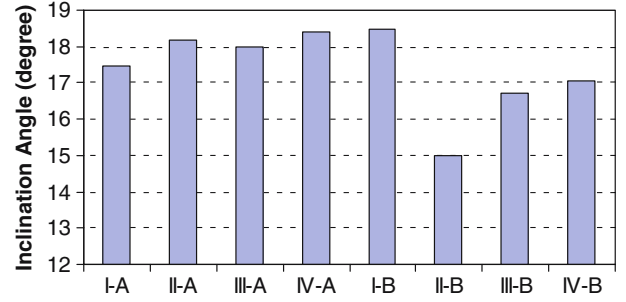

Fig. 15 Average inclination angle of three dimensional bursting events at the bed of vortex chamber for each zone
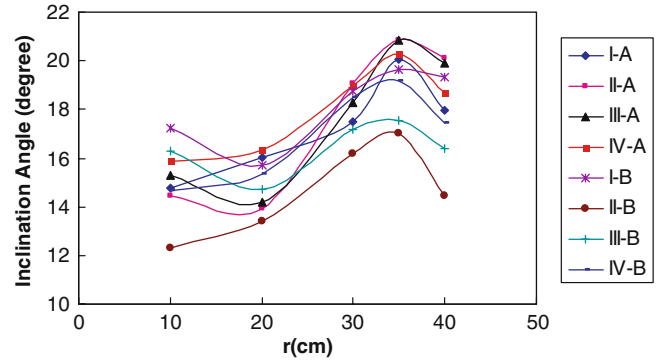

Fig. 16 Variation of inclination angle of each zone toward the periphery wall of the chamber near the bed of vortex chamber

decrease until reaching the periphery wall of chamber. It shows that by increasing tangential velocity toward the center of the chamber, the angle of attack will decrease and the internal sweep events will perform better in moving sediment particles toward the flushing (Fig. 17). Therefore, near the flushing orifice there would be no sediment deposition. Also some relationships were found between the average inclination angle of the zones for each point and their location at the bed of the vortex chamber and they are presented in Table 4.

Table 3 Proposed relationship between the inclination angle of the events in eight bursting zones

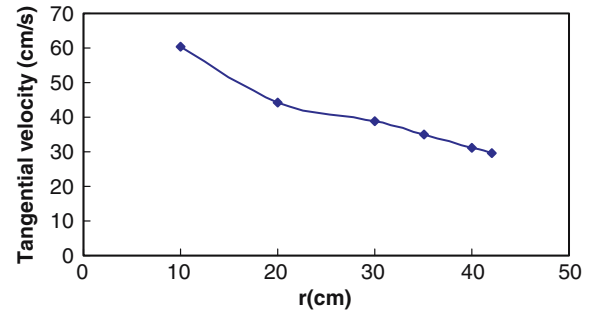| Proposed relationships of class type A	R^2
$\theta_{I-A} = -2.19 - 0.5\,\theta_{II-A} + 0.55\,\theta_{III-A} + 1.02\,\theta_{IV-A}$	0.89
$\theta_{II-A} = -2.75 - 0.52\,\theta_{I-A} + 0.66\,\theta_{III-A} + 0.98\,\theta_{IV-A}$	0.9
$\theta_{III-A} = 4.41 + 0.74\,\theta_{I-A} + 0.85\,\theta_{II-A} - 0.81\,\theta_{IV-A}$	0.83
$\theta_{IV-A} = 2.87 + 0.66\,\theta_{I-A} + 0.61\,\theta_{II-A} - 0.39\,\theta_{III-A}$	0.92
Proposed relationships of class type B	R^2
$\theta_{I-B} = -1.44 - 0.03\,\theta_{II-B} + 0.38\,\theta_{III-B} + 0.82\,\theta_{IV-B}$	0.8
$\theta_{II-B} = -3.39 - 0.04\,\theta_{I-B} + 0.7\,\theta_{III-B} + 0.43\,\theta_{IV-B}$	0.69
$\theta_{III-B} = 6.59 + 0.34\,\theta_{I-B} + 0.46\,\theta_{II-B} - 0.17\,\theta_{IV-B}$	0.66
$\theta_{IV-B} = 3.19 + 0.68\,\theta_{I-B} + 0.27\,\theta_{II-B} - 0.16\,\theta_{III-B}$	0.79

Fig. 17 Variation of tangential velocity toward the periphery wall of the chamber near the bed of vortex chamber

Table 4 Proposed relationships between the inclination angle of the zones and their location at the bed of the vortex chamber

Proposed relationships	R^2
$\theta_{I-A} = 13.71 + 6.34\,(r/R) + 3.91\,\sin\varphi - 2.61\,\cos\varphi$	0.56
$\theta_{II-A} = 11.29 + 11.67\,(r/R) + 3.37\,\sin\varphi - 3.33\,\cos\varphi$	0.68
$\theta_{III-A} = 12.51 + 9.3\,(r/R) + 3.11\,\sin\varphi - 2.48\,\cos\varphi$	0.59
$\theta_{IV-A} = 14.37 + 6.82\,(r/R) + 3.14\,\sin\varphi - 3.02\,\cos\varphi$	0.54
$\theta_{I-B} = 15.07 + 5.79\,(r/R) + 2.02\,\sin\varphi - 3.12\,\cos\varphi$	0.57
$\theta_{II-B} = 11.42 + 6.05\,(r/R) + 1.34\,\sin\varphi - 1.12\,\cos\varphi$	0.27
$\theta_{III-B} = 14.89 + 3.11\,(r/R) + 1.09\,\sin\varphi - 0.64\,\cos\varphi$	0.17
$\theta_{IV-B} = 13.9 + 5.35\,(r/R) + 1.28\,\sin\varphi - 2.55\,\cos\varphi$	0.47

4 Conclusions

In this study, three dimensional quadrant analysis of the velocity fluctuations was used to find the entrainment and deposition of sediment particles at the bed of a vortex chamber. It was found that three dimensional quadrant analysis of bursting process is capable of recognizing the susceptible regions for sediment accumulation at the bed of vortex chamber. It was also concluded that the zones of class A, and in particular the internal sweep events are responsible for sediment transport toward the center of the chamber and the flushing orifice. The events that occur inside the zones of class B cause the sediment particles to move toward the wall of the chamber. Also the average inclination angle of the bursting events in each zone shows that at the region where a great amount of sediment was piled up, the bursting events have the higher inclination value. It was also found that by moving toward the center of the chamber, as the tangential velocity increases, the rate of inclination of the events decrease.

References

Drake TG, Shreve RL, Dietrich WE, Whiting PJ, Leopold LB (1988) Bed load transport of fine gravel observed by motion-picture photography. J Fluid Mech 192:193–217

Grass AJ (1971) Structural features of turbulent flow over smooth and rough boundaries. J Fluid Mech 50(2):233–255

Hinze JO (1975) Turbulence 2nd Edition. McGraw-Hill

Keshavarzi AR (1997) Entrainment of sediment particles from a flat mobile bed with the influence of near-wall turbulence PhD Thesis. University of New South Wales, Australia

Keshavarzi AR, Ball JE (1997) An analysis of the characteristics of rough bed turbulent shear stress in an open channel flow. J Stochastic Hydrol and hydraulics 11(3):193–210

Keshavarzi AR, Ball JE (1999) An application of image processing in the study of sediment motion. J Hydra Res 37(4):559–576

Keshavarzi A, Shirvani A (2002) Probability analysis of instantaneous shear stress and entraind particles from the bed. CSCE/EWRI of ASCE Environmental Engineering Conf, Niagara

Kline SJ, Reynolds WC, Schraub FA, Runstadler PW (1967) The structure of turbulent boundary layers. J Fluid Mech 30(4):741–773

Nakagwa H, Nezu I (1978) Bursting phenomenon near the wall in open channel flow and its simple mathematical model. Mem Fac Eng Kyoto University, Japan XL(4) 40:213–240

Nelson JM, Shreve RL, Mclean SR, Drake TG (1995) Role of near-bed turbulence structure in bed load transport and bed form mechanics. Water Res Res 31(8):2071–2086

Nezu I, Nakagawa H (1993) Turbulence in open channel flows. IAHR Monograph, Balkema, Rotterdam

Nychas SG, Hershey HC, Brodkey RS (1973) A visual study of turbulent shear flow. J Fluid Mech 61:513–540

Offen GR, Kline SJ (1975) A proposed model of the bursting process in turbulent boundary layers. J Fluid Mech 70:209–228

Papanicolaou AN, Diplas P, Evaggelopoulos N, Fotopoulos S (2002) Stochastic incipient motion criterion for spheres under various bed packing conditions. J Hydraulic Eng ASCE 128(4):369–380

Sontek ADV Operation Manual (1997) Firmware Version 4.0. Sontek:San Diego

Thorne PD, Williams JJ, Heathershaw AD (1989) In situ acoustic measurements of marine gravel threshold and transport. Sedimentology 36:61–74

Townsend AA (1956) The structure of turbulent shear flow. Cambridge University Press, Cambridge

Yalin MS (1992) River mechanics. Pergamon Press Ltd, Oxford

Yen BC (2002) Stochastic inference to sediment and fluvial hydraulics. J Hydraulic Eng, ASCE 128(4):365–367